Chapter 1

A Practical Review of Microrheological Techniques

Bradley W. Mansel, Stephen Keen, Philipus J. Patty,
Yacine Hemar and Martin A.K. Williams

Additional information is available at the end of the chapter

http://dx.doi.org/10.5772/53639

1. Introduction

Microrheology is a method for the study of the viscoelastic properties of materials [1, 2]. It has many potential benefits including requiring only microlitres of sample and applying only microscopic strains, making it ideal for costly, rare or fragile samples. Ever since the earliest papers began emerging in the biophysical arena some ten to fifteen years ago [3,4], to more current publications [5-8] fascinating insights into the material properties of the cell and its constituent biopolymers have been revealed by microrheological studies. It can extract information about the underlying heterogeneities in soft materials of interest, and can measure viscoelastic properties to high frequencies compared to traditional rheological measurements [9]. This paper reviews the limits of speed and accuracy achievable with current advances in instrumentation, such as state-of-the-art correlators and cameras, by directly comparing different methodologies and equipment.

2. Basic principles

2.1. Extracting traditional rheological parameters

To use microrheology to obtain the traditional storage and loss moduli, (G′, G′′), of complex soft materials of interest, the mean square displacement (MSD) of microscopic tracer particles must be measured, defined in three dimensions as:

$$\left\langle \Delta r^2(\tau) \right\rangle = \left\langle \left[x(t+\tau) - x(t) \right]^2 + \left[y(t+\tau) - y(t) \right]^2 + \left[z(t+\tau) - z(t) \right]^2 \right\rangle \quad (1)$$

where, τ is the lag time, t is the time and x, y and z represent position data [10]. There are a number of experimental techniques to measure the MSD, each with its own advantages and disadvantages that will be described in due course.

If a material is purely viscous, the MSD of an ensemble of thermally-driven tracer particles will increase linearly with time, yielding a logarithmic plot having a slope of one. In contrast, tracers embedded in a purely elastic material will show no increase in the MSD with time and the particle's location will simply fluctuate around some equilibrium position. While these two limiting cases are intuitive many materials of interest, particularly in the biophysical arena, are viscoelastic, both storing and dissipating energy as they are deformed. This is signaled by a slope between the extreme cases of zero and one on a logarithmic plot of MSD versus time. Additionally materials often display differing viscoelastic properties on different time-scales so that the slope of such a plot can change throughout the experimentally observed range. Indeed, the range of lag times over which the MSD is measured is equivalent to probing the viscoelastic properties as a function of frequency. Whilst the basic idea of using the dynamic behavior of such internal colloidal probes as an indication of the viscoelasticity of the surrounding medium has a long history, it took the relatively recent availability of robust numerical methods to transform the raw MSD versus time data into traditional viscoelastic spectra to drive the field forwards [10].

Tracer particles embedded in a **purely viscous medium** have an MSD defined by:

$$\left\langle \Delta r^2 \left(\tau \right) \right\rangle = 2dD\tau \tag{2}$$

where τ is the lag time, d is the dimensionality and D is the diffusion coefficient, which is defined by the ratio of thermal energy to the friction coefficient, as embodied by the famous Einstein-equation:

$$D = \frac{k_B T}{f} \tag{3}$$

where, T, is the temperature and f is the friction coefficient. For added spherical tracers in low Reynolds number fluids, f can be calculated by the Stokes drag equation for a sphere:

$$f = 6\pi\eta R \tag{4}$$

where η is the viscosity of the surrounding material and R, the radius of the tracer.

Tracer particles embedded in a **viscoelastic medium** do not have such a simple relation between the MSD and diffusion coefficient. However, a Generalized Stokes-Einstein Relation (GSER) can be used, that accommodates the viscoelasticity of a complex fluid as a frequency dependent viscosity, yielding [1, 10, 11]:

http://dx.doi.org/10.5772/53639

$$\tilde{G}(s) = \frac{k_B T}{\pi a s \left\langle \tilde{r}^2(s) \right\rangle} \tag{5}$$

where $\langle \tilde{r}^2(s) \rangle$ is the Laplace transform of the MSD and, $\tilde{G}(s)$ is the viscoelastic spectrum as a function of Laplace frequency, s [1]. This relationship provides a method to quantify the rheological properties of a viscoelastic medium and calculate the storage and loss modulus from the MSD measurement. Many methods are available to implement this scheme, although the numerical method of Mason and Weitz is possibly the most popular method, due to its simplicity and ability to handle noise [10]. Briefly, the MSD plot is fitted to a local power law and the logarithmic differential is then calculated:

$$\alpha(\tau) = \frac{d \ln \left\langle \Delta r^2(\tau) \right\rangle}{d \ln(\tau)} \tag{6}$$

which is used with, Γ, the gamma function in an algebraic form of the GSER:

$$\left| G^* \right| \approx \frac{k_B T}{\pi a \left\langle \Delta r^2 \left(\tau = 1/\omega \right) \right\rangle \Gamma \left[1 + \alpha \left(\tau = 1/\omega \right) \right]} \tag{7}$$

Finally, defining $\delta(\omega)$ as:

$$\delta(\omega) = \frac{\pi}{2} \frac{d \ln \left| G^*(\omega) \right|}{d \ln \omega} \tag{8}$$

then the storage and loss moduli with respect to frequency can be obtained:

$$G'(\omega) = \left| G^*(\omega) \right| \cos\left(\delta(\omega) \right) \tag{9}$$

$$G''(\omega) = \left| G^*(\omega) \right| \sin\left(\delta(\omega) \right) \tag{10}$$

Thus, with the framework of microrheology clear and modern methods in place to obtain traditional viscoelastic spectra from the movement of internalized tracer particles, the discussion switches to reviewing experimental methods for the extraction of their mean squared displacement.

2.2. Measuring the MSD

In order to facilitate the review of the available techniques four different modern techniques have been used to measure the positions of micron sized particles embedded in soft materials, namely: Dynamic Light Scattering (DLS), Diffusing Wave Spectroscopy (DWS), Multiple Particle Tracking (MPT), and probe laser tracking with a Quadrant Photo Diode (QPD) and the use of Optical Traps (OT).

2.3. Light scattering techniques

Dynamic light scattering (DLS) techniques for microrheology use a coherent monochromatic light source and detection optics to measure the intensity fluctuations in light scattered from tracer particles of a known size, which are embedded in a material of unknown viscoelastic properties. Light passing through the sample produces a speckle pattern that fluctuates as the scattering probe moves. Thus, by measuring the intensity fluctuations of the dynamic speckle, at a single spatial position, information about the diffusion of particles in the sample can be gathered [12]. A correlation function is defined by:

$$g^{(2)}(\tau) = \frac{\langle I(t) I(t+\tau) \rangle}{\langle I(t) \rangle^2} \tag{11}$$

With τ, the lag time, t the time and the angular bracket denoting a time average. For ergodic samples the auto-correlation function can be simply converted to the so-called field auto-correlation function, $g^{(1)}$, using the Siegert relation:

$$g^{(2)}(\tau) = 1 + \beta \left| g^{(1)}(\tau) \right|^2 \tag{12}$$

The coherence factor, β, in this relationship, is related to the experimental setup, and for a properly aligned system should be close to unity. DLS uses a sample containing a low number of probe scatterers to ensure that each photon exiting the sample has been scattered only a single time. Using recently developed techniques such as multiple scattering suppression [13] one can still extract some information if multiple scattering cannot be avoided, but these are not commonly used as sample optimization can often provide a simpler solution. Central to DLS experiments is the scattering vector defined by:

$$q = \frac{4n\pi}{\lambda} \sin\left(\frac{\theta}{2}\right) \tag{13}$$

where λ represents the wavelength of the incident laser light, n, the refractive index of the medium surrounding the scatterer and θ the angle the incident beam makes with the detec-

http://dx.doi.org/10.5772/53639

tor. Ultimately, for traditional DLS experiments, the q vector must be known to extract information about the displacements made by the particles. For more information see Dasgupta [14] or Pecora [12].

Practically, light emitted from a continuous wave, vertically-polarized laser is directed through the sample held in a goniometer. Using a polarized laser combined with a crossed polarizer on the detection optics helps to reduce the chance of light that has not been scattered entering the detection optics, which helps improve the signal. As well as providing angular control the goniometer typically has a bath surrounding the sample that is filled with a fluid of a similar refractive index to the cuvette in which the sample is housed, to help eliminate light reflections from the surface. In the case of the DLS setup used in our studies, detection optics in the form of a gradient index (GRIN) lens directs photons scattered at a particular angle into a single-mode optical fiber that incorporates a beam splitter. The two beams thus produced are taken to two different photo multiplier tubes (PMTs) that produce electronic signals. These are interrogated by a correlator interfaced to a computer that converts fluctuations in the scattered light falling onto the PMTs into a correlation function. When two photomultiplier tubes are used the *cross*-correlation function can be formed, as opposed to an *auto*-correlation function that can be measured with a single PMT. Cross correlation help circumvent dead time in the electronics as well as helping eliminate after-pulsing effects. A schematic of a typical experimental setup is shown in figure 1(a).

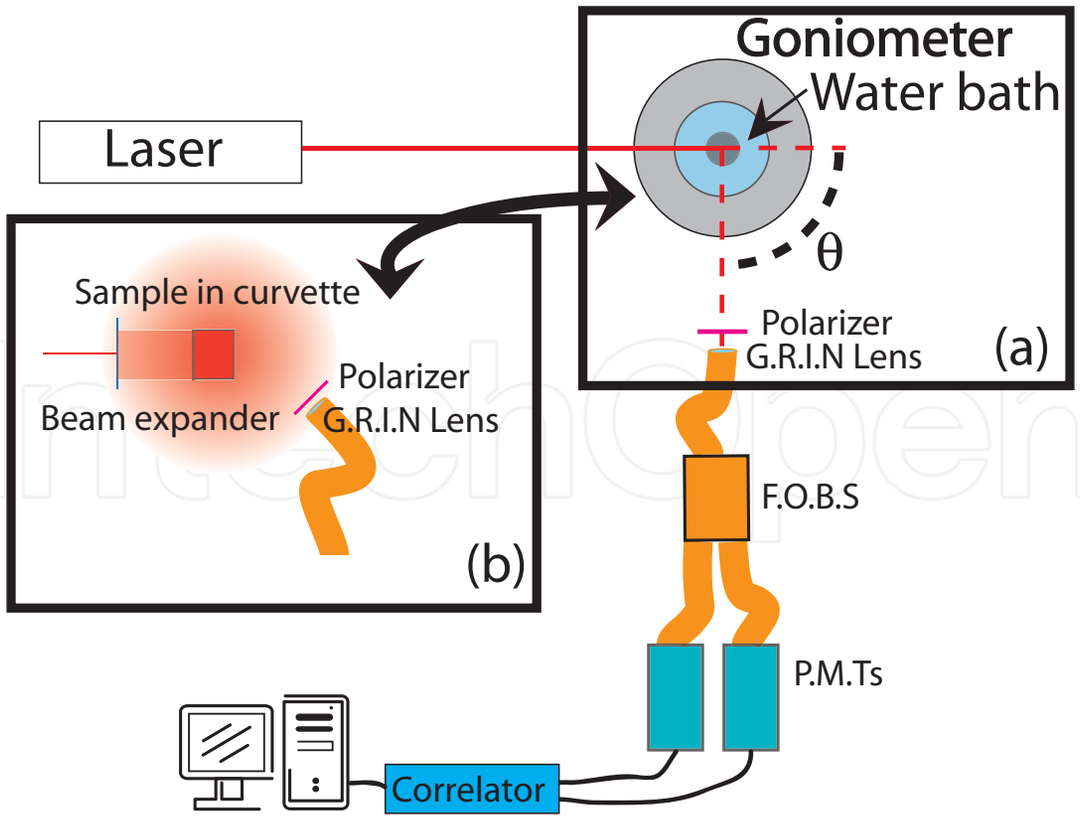

Figure 1. Schematic of light scattering apparatus used, showing a) goniometer for DLS and b) the DWS setup.

In DLS, where single scattering events dominate, the decay of the field correlation function, $g^{(1)}$, is related to the diffusion of the particles in the sample by:

$$g^{(1)}(\tau, q) = \exp(-Dq^2\tau) \tag{14}$$

where τ represents the lag time, q, the scattering vector and D the diffusion coefficient which, by equation (2) can be written as [12]:

$$g^{(1)}(\tau, q) = \exp\left(\frac{-q^2\left\langle \Delta r^2(\tau)\right\rangle}{6}\right) \tag{15}$$

By inverting this equation one obtains the MSD versus lag time directly from the field correlation function.

Diffusing Wave Spectroscopy: At high frequencies DLS is limited by the sensitivity of the correlator. This limitation can be overcome by adding many scatterers to the sample. The light now diffuses through the sample taking a random walk with mean-free path, l [15]. The diffusion of light through the sample means that even if each individual scatterer was only to move a very small amount, the overall path that the light travels is changed very dramatically, resulting in a much higher sensitivity than DLS. However, when making measurements in materials with a very large number of scatterers a statistical approach must be used to derive the form of the correlation function. To ensure the accuracy of the statistical approach the number of scatterers must be large enough so that the photon paths can be themselves described by a random walk. Light scattering in this high scattering limit is known as Diffusing Wave Spectroscopy (DWS) [15].

The equipment used for DWS is very similar to that used for DLS. The main difference is that no goniometer is required as, provided that all the photons studied have traversed the cell, there is no angular dependence of the intensity of scattered light. Additionally the incident beam is first expanded to distribute the intensity of the light across the width of the sample cuvette, (in the case described here to around 8 millimetres). Otherwise, as in DLS, a continuous wave, vertically polarized, laser is used as the light source; the scattered light is coupled to a single mode optical fibre using a GRIN lens; split by a single mode fiber-optic beam-splitter (FOBS) and sent to two PMTs. The correlation function is then calculated using a cross-correlation method in software on a standard personal computer. A schematic of the experimental setup used here can be seen in figure 1 (b).

The measurement of the length a photon must travel before its direction is completely randomized, l^*, is fundamental to DWS. Firstly, comparing it to the pathlength of the cell reveals if the number of scatterers present in a sample is large enough to validate the diffusive criterion, and secondly, it is needed in order to extract the MSD from the correlation function. l^*, being at least four times smaller than the thickness of the sample ensures that

the light is strongly scattered, producing statistically viable results. To calculate the MSD in transmission geometry, with uniform illumination over the face of the sample, an inversion is performed on the following equation [15]:

$$g^{(1)}(\tau)=\frac{\left(\frac{L/l^*+4/3}{z_0/l^*+2/3}\right)\sinh\left(\frac{z_0}{l^*}\sqrt{k_0^2\langle r^2\rangle}\right)+\frac{2}{3}\sqrt{k_0^2\langle r^2\rangle}\cosh\left(\frac{z_0}{l^*}\sqrt{k_0^2\langle r^2\rangle}\right)}{\left(1+\frac{8t}{3\tau}\right)\sinh\left(\frac{L}{l^*}\sqrt{k_0^2\langle r^2\rangle}\right)+\frac{4}{3}\sqrt{k_0^2\langle r^2\rangle}\cosh\left(\frac{L}{l^*}\sqrt{k_0^2\langle r^2\rangle}\right)} \tag{16}$$

Here L represents the thickness of the sample and l^* the transport mean free path of the medium. It is assumed that the source of diffusing intensity is a distance, z_0, inside the sample, which is routinely assumed to be equal to l^*. k_0 is the wave vector of the incident light, equal to $2\pi\lambda$. For a detailed description on the theory of DWS and the mathematics behind equation (16) see chapter 16 of *Dynamic light scattering: The Method and Some Applications* edited by Wyn Brown, which covers this extensively [15].

Summary: Generally light scattering techniques have the advantage that they have a low setup cost, are well known and produce reliable results. DLS, one of the more common light scattering techniques, cannot measure to the high frequencies of DWS and also has a slightly higher setup cost as a goniometer is required for angular control. However, if many measurements can be taken and averaged, DLS can produce very consistent results, and if the scattering angle is reduced it is possible to obtain particle dynamics out to tens of seconds. DWS is also a robust, well proven technique that can achieve higher frequency measurements than any other method, due to a small displacement of the bead causing an additive effect in each successive scatter through the sample. Traditional light scattering experiments do not however have the ability to extract any information about the homogeneity of the sample, although this can be accomplished to some extent using modified techniques such as multispeckle DWS, where the PMT is replaced by a camera [13, 16].

2.4. Real space tracking techniques

Multiple particle tracking typically consists of visually tracking tens to hundreds of probe particles embedded in the material to be studied [9]. Commonly, an epifluorescence microscope with a CCD or CMOS camera is used to record a series of images of fluorescent tracer particles as they undertake random walks due to Brownian motion. Fluorescence microscopy has many advantages over simple bright field microscopy; it produces images with the particles represented as bright spots on a dark background, facilitating the use of many different tracking algorithms, and allows the position of particles smaller than the wavelength of light to be obtained. Image series taken from the chosen microscopy technique are subsequently processed using tracking software, turning the images into a time-course of x-y coordinate data for each particle. From this data the MSD can be calculated and hence the rheological information extracted. MPT is mainly limited by the temporal resolution of the

camera (typically 45 Hz), meaning that lower frequency rheological information is accessible when compared with other light-scattering based microrheology techniques. It has advantages however of measuring information about the spatial homogeneity of the sample, and is one of the few techniques capable of studying the viscoelastic properties of living samples where, for example, naturally occurring particles (liposomes and organelles) might be tracked.

Information about spatial homogeneity:
A plot of the probability of displacements of a certain value observed at each time lag gives an indication of homogeneity. If the sample is homogenous then one would expect this to result in a Gaussian function centred on the origin at each time lag, with the variances of the distributions being the MSDs. The plotting of the frequency with which a measured displacement falls in a particular displacement-range is known as a Van Hove plot [17], and is shown for particles diffusing in water in figure 2.

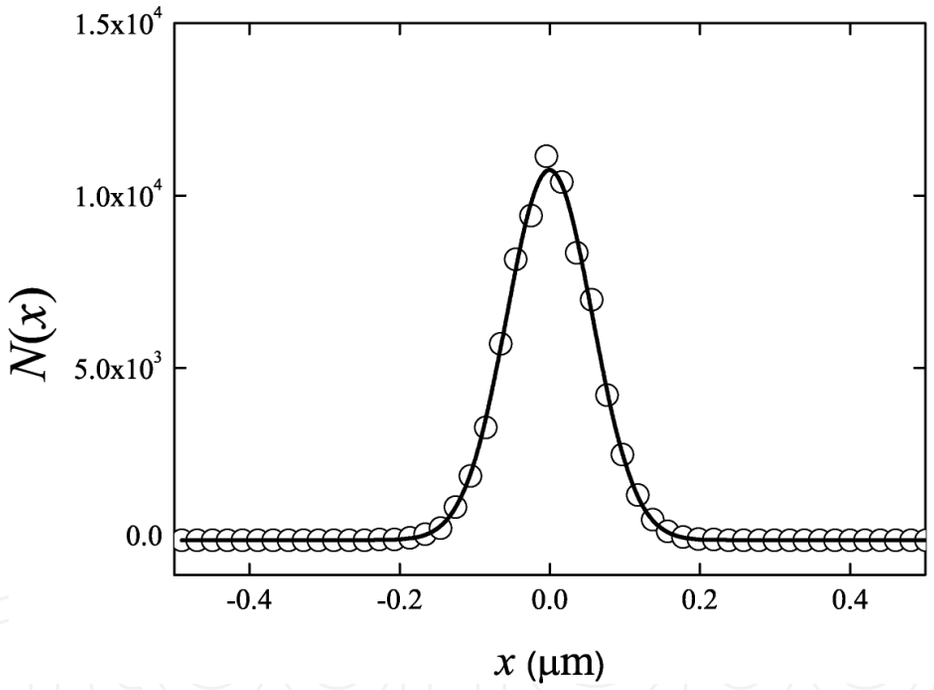

Figure 2. A Van Hove plot measured for 505nm polystyrene fluorescence particles diffusing in a glycerol water mixture, a homogenous medium, as can be seen by a good agreement to a Gaussian fit (solid line). Data obtained using a CMOS camera at 45Hz.

If significant heterogeneities exist then the Van Hove function will be non-Gaussian, indicating that the differences in the distances travelled by different beads in the same time does not simply represent the sampling of a stochastic process, but that differences in the local viscoelastic properties exist. The Van Hove plots of such heterogeneous systems can be quantified by a so-called non-Gaussian parameter that reports how much the ratio of second to fourth moments of the distribution differs from the Gaussian expectation [18, 19]. Infor-

mation about the underlying structure of the sample can also be extracted by observing the behavior of the MSD when probe particles of different sizes are used [20].

The so-called one-point microrheology (OPM) described thus far simply extracts the displacements of each probe particle by comparing their co-ordinates in time-stamped frames recorded by the camera using a tracking algorithm. This is the simplest form of analysis and is often sufficient. However, the results can be highly dependent on the nature of interactions existing between the tracer particles and the medium, and effects of any specific binding, or depletion interactions can produce spurious measurements of the viscoelastic properties of the medium [21]. That is, OPM can be thought of as a superposition of the bulk rheology and the rheology of the material at the particle boundary [22]. With video-microscopy, where multiple probe-particles are tracked simultaneously, a method to overcome these difficulties has been developed, known as two-point microrheology (TPM). TPM only differs in the way the data is analysed, in that, rather than just looking at one particle TPM measures the cross-correlation of the movement of pairs of particles [22]. In some cases TPM has been shown to measure viscoelastic properties in better agreement with those measured using a bulk rheometer, due to the elimination of dependence on particle size, particle shape, and coupling between the particle and the medium [23]. TPM is a fairly intuitive technique if the two limiting cases are considered; the probe particles in an elastic solid will exhibit completely correlated motion throughout the sample, while in a simple fluid they would exhibit very little correlated motion. In between these extremes the viscoelasticity can be quantified by knowledge of the distance between particles, the thermal energy and the cross-correlation function [24]. While it does have potential advantages, two-point microrheology is very susceptible to any drift or mechanical vibration; which appears as completely correlated motion [24]. If the material of interest is homogenous, incompressible, isotropic on length-scales significantly smaller than the probe particle, and connected to the tracers by uniform no-slip boundary conditions over the whole surface, then the one- and two- point MSDs should be equal [24].

To perform two-point microrheology first the ensemble average tensor product is calculated:

$$D_{\alpha\beta}(r,\tau) = \left\langle \Delta r_\alpha^i(t,\tau)\Delta r_\beta^i(t,\tau)\delta\left(r - R^{ij}(t)\right)\right\rangle_{i\neq j,t} \tag{17}$$

where i and j label different particles, and label different coordinates, and R^{ij} is the distance between particle i and j. The distinct MSD can be defined by rescaling the two-point correlation tensor by a geometric factor [22-24]:

$$\left\langle \Delta r^2(\tau)\right\rangle_D = \frac{2r}{a} D_{rr}(r,\tau) \tag{18}$$

where a is the diameter of the probe particles. Further information on the mathematics behind the method can be obtained from Crocker (2007) [24] and Levine (2002) [23].

Tracking software: A plethora of different programs and algorithms exist to track objects in successive images. Both commercial and freeware programs exist. Commercial software such as Image Pro Plus, can track images straight out of the box with little fuss, although it is reasonably costly. One can also write their own program to cater to their own needs, and kindly many research groups have made free software available that generally works as well as many commercial packages. There are four main tracking algorithms, namely: centre of mass, correlation, Gaussian fit and polynomial fit with Gaussian weight. Ready to use programs are available on the following web pages:

http://www.physics.emory.edu/~weeks/idl/ This web page is a great resource with links to many different programs written in many different programming languages.

http://physics.georgetown.edu/matlab/ This code uses the centroid algorithm for sub-pixel tracking, it is the code used for the majority of the particle tracking in this work. Some knowledge of programming in MATLAB is needed to implement the code.

http://www.people.umass.edu/Kilfoil/downloads.html This resource has code available for calculating the MSD, two-point microrheology, and many other useful programs implemented in MATLAB.

http://www.mosaic.ethz.ch/Downloads/ParticleTracker This page has links to a 2D and 3D particle tracking algorithm, as published in [25]. The code is implemented using ImageJ a popular Java-based open source image processing and analysis program.

http://www.mathworks.de/matlabcentral/fileexchange/authors/26608 Polyparticle tracker uses a polynomial fit with Gaussian weight. This powerful tracking algorithm has a good graphical user interface and is easy to implement. Details of the algorithm can be viewed in the following publication [26].

Theoretically it can be seen that the selection of tracking algorithm could play a large role in multiple particle tracking experiments. In reality the differences in performance between different tracking algorithms can largely be overcome by optimizing the experimental setup. Indeed Cheezum (2001) [27] have shown that at a high signal-to-noise ratio the different tracking algorithms produce very similar bias and standard deviations. The lower limit where differences in the algorithms do become important is a signal-to-noise of around 4, which roughly corresponds to imaging single fluorescent molecules. The fluorescent microspheres imaged in multiple particle tracking experiments are many tens of times brighter than the background fluorescence, generally providing a high signal-to-noise. Additionally, modern cameras have photo-detector arrays consisting of many megapixels, resulting in a particle diameter in the order of tens of pixels, so that effects from noise on the edge of a particle often have little effect. Oscillation and drift in an experimental setup can however create large sources of error and often are the hardest errors to remove. For a more in depth description see references Rogers (2007) [26] and Cheezum (2001) [27]. Errors in particle tracking can be placed in 4 different categories: Random error, systematic error, dynamic error and sample drift. A thorough discussion is given in Crocker (2007) [24] and further precise methods with which to estimate the static and dynamic errors present in particle tracking are given by Savin (2005, 2007) [28, 29]. Practically multiple experimental techni-

ques are often used and the comparison of results quickly reveals if significant errors in the MPT are present.

Optimizing experimental set-up for microscope based experiments: The camera used for MPT is the central apparatus limiting the temporal and spatial resolution. Current CMOS technology allows the fastest frame rate of any off-the-shelf camera designed for microscopy [30, 31]. The main problem with this technology is the sensitivity, although these issues are beginning to be addressed [32]. Cameras with a high sensitivity, large detector size, higher speed and small pixel size can obtain a larger amount of information from the sample. To supply the tracking algorithm with enough information to calculate the position of a probe particle to sub-pixel accuracy, the particle must be represented by a sufficient number of pixels. The size representation of fluorescent particles is dependent on the size of the particles, the intensity of the excitation fluorescent lamp, the size of each pixel on the sensor, and the magnification of the objective lens used. The strength of the fluorescent lamp that can be used is ultimately limited by the speed at which it photo-bleaches the fluorophore. One possible method to overcome the photo-bleaching difficulties is to use quantum dots.

Magnification: For high signal-to-noise applications, it is advantageous to have the highest possible magnification, resulting in the particles being represented by the maximum number of pixels, and so enhancing the accuracy of the tracking algorithm subsequently applied [33]. However, as the magnification is increased the illumination of each pixel decreases as the square of the magnification. This results in a decrease in the signal-to-noise proportional to the magnification, if the illumination is not increased [33] and therefore for low signal-to-noise applications, the highest possible magnification will not always result in the best image sequence for tracking. As a result care must be taken in selecting the correct magnification objective lens. A simple method to check that the selected objective is of the correct magnification before recording an image sequence is to record a single image, then using an image analysis program such as ImageJ (http://rsbweb.nih.gov/ij/) to find the brightness of an individual pixel on a particle. This can then be compared to the background brightness of the image. By comparing the two intensity values one can roughly estimate the signal-to-noise. If the signal to noise is too low (< ~10) then a lower power objective lens can be chosen. This basic method will suffice to quickly give an indication of what objective is appropriate for the sample. A lower magnification objective will also result in a larger field of view in the sample, thus, the positions of more individual particles can be measured, and better statistics of the ensemble averaged MSD will result.

Numerical aperture: A high numerical aperture (NA) objective lens creates a higher resolution image than the equivalent lower NA objective lens. This would suggest that a high NA objective lens would create a superior image for tracking, although, a high NA objective also results in a small point-spread function, meaning a smaller image. In reality these two competing effects relating to the NA lens used usually cancel out. A simple calculation shows that if the signal-to-noise is high (around 30) then there is no effect of the NA used. No relation between the NA and accuracy of tracking was found in an experiment performed using different tracking algorithms and comparing data for a 0.6 NA and 1.3 NA lens [33].

Allan variance: If no drift is present in an experimental setup, a very unlikely situation, then the longer the experiment is run the better the accuracy of the measurement. However, if drift is present, as in nearly every experimental setup, running the experiment for the longest duration will not result in the highest accuracy measurement, it will actually result in a worse measurement than if the measurement was taken for a shorter duration. One can check the optimum length of time for which to record an experiment by using the Allan Variance. Defined as:

$$\sigma_x^2(\tau) = \frac{1}{2}\left\langle \left(x_{i+1} - x_i\right)^2 \right\rangle_\tau \tag{19}$$

where τ is the time lag, x_i is the mean over the time interval defined as $(\tau) = f_{acq} m$, where m is the number of elements in that interval acquired at f_{acq}, and the angle brackets denote arithmetic mean [34]. Most commonly the Allan variance is used in optical tweezers experiments, and the tracking performed using a Quadrant Photodiode (QPD) discussed in the following section, although with modern CMOS cameras approaching the kilohertz regime one can optimize particle-tracking experiments in this way. The Allan variance can be seen in figure 3 to decrease as the number of measurements (number of lag times evaluated) increases, until such long lag times are used that drift becomes a significant effect on the measurement.

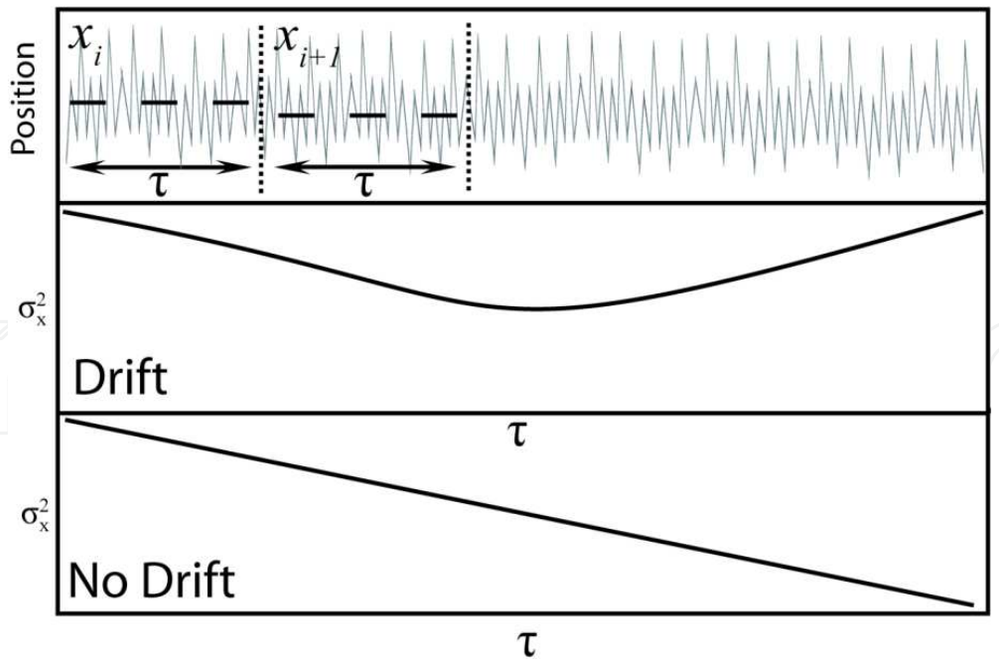

Figure 3. Schematic showing the relation between a particles mean position and the Allan Variance. It can be seen that in a perfect experiment, with no drift, the Allan variance decreases for the duration of the experiment, but where drift is present the Allan variance has a minimum corresponding to when the effects of sampling statistics and drift are balancing out.

2.5. QPD measurements using optical traps

The movement of individual probe particles can also be tracked using a probe laser and a quadrant photodiode (QPD) (a photodiode that is divided into four quadrants). A probe laser is used to scatter light from the selected particle and this produces an interference pattern that is arranged to fall on the QPD. Two output voltages are produced from the difference- signals generated by light falling on different quadrants and therefore any movement of the interference pattern on the QPD is detected by a change in output voltages. Thus, if the probe particle is located between the laser and QPD, any motion of the particle will be detected. Once calibrated these recorded voltages correspond directly to a measurement of the x and y co-ordinates of the probe particle - so that ultimately the output is equivalent to that which would be obtained by a video-microscopy tracking experiment. While the calibration requires an extra step in the measurements, a QPD has the advantage that measurements are not limited by a camera frame rate and for commercial QPDs can be taken on the order of tens of microseconds, subsequently giving access to rheological information up to the 100 kHz regime, albeit one probe particle at a time.

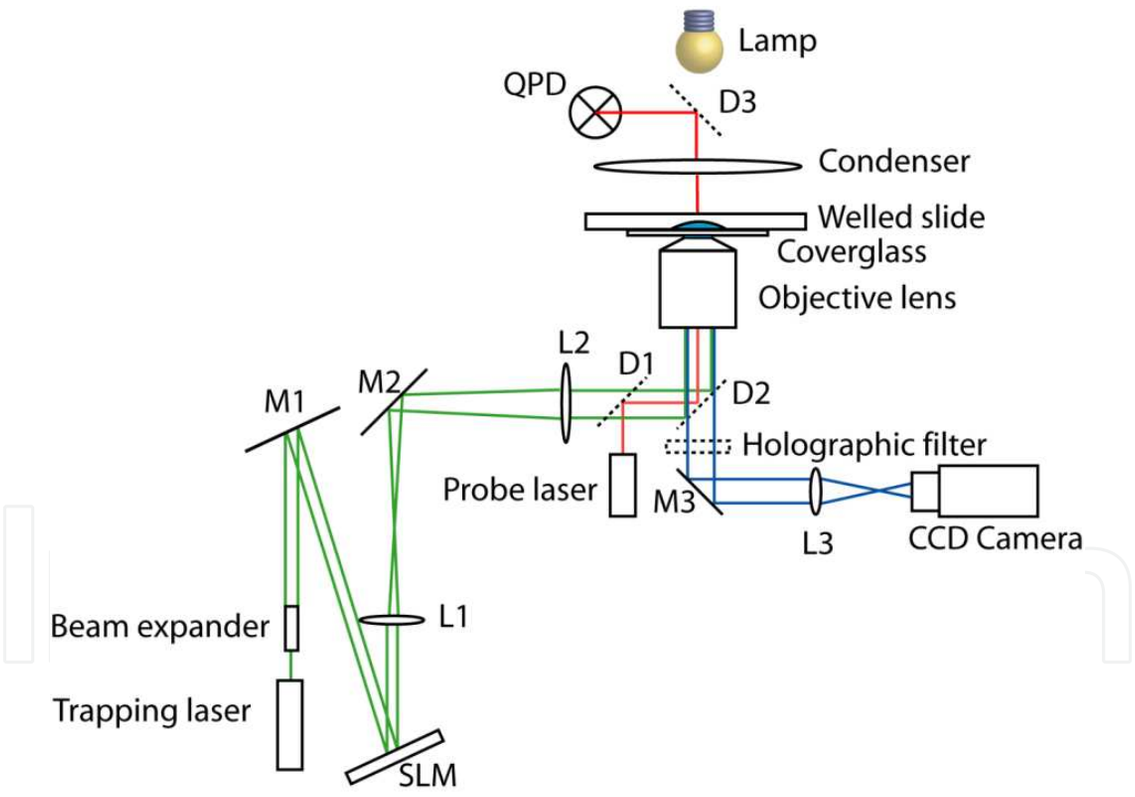

Figure 4. Schematic of the microscope and optical tweezers apparatus.

There is, however, an additional complication in making such measurements. Clearly a fixed QPD is limited in the maximum particle displacement it can measure and as probe particles are diffusing in 3 dimensions it is essential to provide a mechanism that ensures the particle being tracked stays within the range of the QPD. This can be carried out with an optical tweezers ar-

rangement that uses a tightly focused higher-power laser to hold and manipulate micron-sized particles [35-37]. Figure 4 shows a typical holographic optical tweezer setup (HOT) that employs a spatial light modulator (SLM), which provides the ability to make multiple steerable traps and move objects in three dimensions using a single laser, in real time [38, 39].

Optical traps [40] formed by such an arrangement can be utilized to restrict larger-scale movements of probe particles so they stay in the detection region of the QPD / laser apparatus - essentially fencing them in, while leaving the smaller scale Brownian-motion unperturbed. At longer time lags the effect of the trap can be seen in the MSD plot, as a plateau indicating the effect of the trap, as shown in figure 5.

Calibration of the raw photodiode voltages in order to obtain actual bead displacements are routinely carried out by moving a probe particle a set distance across the QPD detection area. This can be carried out either by locating a particle that is stuck to the coverslip of the sample cell and translating the chamber a known amount using a piezo-electric stage; or by moving a particle using a pre-calibrated optical trap. An average piezoelectric stage currently available for microscopy is able to provide nanometer resolution to displacements up to 300 microns.

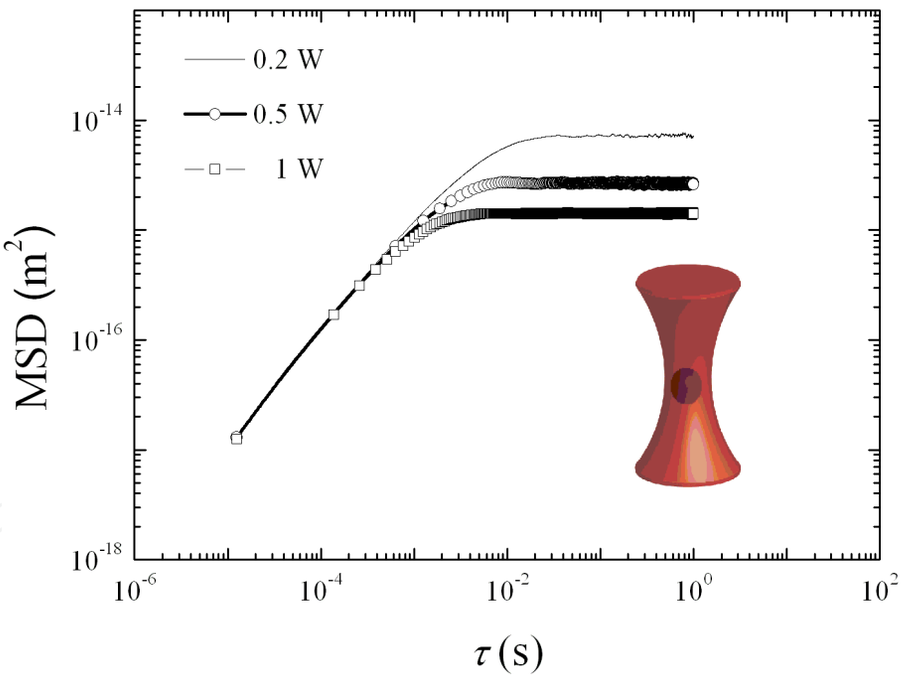

Figure 5. MSD plot of a particle undertaking Brownian motion within optical traps formed with three different laser intensities. The insert shows a particle optically trapped.

2.6. Standard experimental studies

Having described the setup and calibration of four microrheological techniques, results obtained from 3 different fluids are described and compared. Water, a glycerol-water mixture, and several polyethylene oxide (PEO) solutions were utilized to provide three different en-

vironments, namely; low viscosity, high viscosity and viscoelastic fluids, to test and compare the different methods. Such samples are standards that can be quickly used to ensure the proper functioning of the equipment and analysis before more complex biological systems are investigated.

Samples:*Water* has a lower viscosity than most biological materials of interest; and thus provides a good test of how the methodologies cope with fast particle dynamics. *Glycerol* is a homogenous, purely viscous fluid and was used in combination with water (results shown here for 62 wt%) to generate a highly viscous solution. Solutions were made by mixing glycerol (99.9% from Ajax Laboratory Chemicals) and MilliQ water, using a magnetic flea, for approximately 2 hours. *PEO*, an electrically-neutral water-soluble polymer available in a range of molecular weights was used to generate a viscoelastic polymer solution. PEO starts to exhibit viscoelasticity at concentrations higher than the overlap concentration (approximately 0.16 wt% for the 900 kDa PEO samples used in the following experiments). Solutions were made by adding dry PEO powder (Acros Organics) in MilliQ water, and then slowly mixing over approximately a 7 day period to help homogenize the solution. Solutions were prepared at 2.2 wt% and 4 wt%, around 14 and 25 times the overlap concentration, to ensure significant viscoelasticity [14]. The mesh size of PEO solutions at these concentrations have been calculated to be the order of a few nanometres. As there is little evidence of surface effects between the particles and these solutions, and the solution is then homogenous on the length scale smaller than the particle size, it was expected that the one-and two-point microrheology should produce very similar results, and as such the system forms an ideal test of those two methodologies.

Probe Particles: DWS measurements require a high bead concentration producing a turbid solution and ensuring strong multiple scattering. On the other hand, optical tweezers experiments and DLS measurements require that the concentration of particles in the solution is very low. For optical tweezers one must ensure that that there is only one particle present in the imaging plane, any more and there is a chance that a second additional particle might get sucked into the trap, and as discussed DLS requires that photons only be scattered a single time. For DLS and DWS polystyrene particles are chosen due to their low density and good scattering properties. Silica particles are used for optical tweezers due to the high refractive index of silica, which ensures a strong trapping force. DLS and DWS experiments were carried out for all samples with solid polystyrene probe particles (Polysciences) at concentrations of 0.01% and 1%, respectively. Solutions for optical tweezers and MPT experiments were made to concentrations of 10^{-6} % solid silica (Bangs Laboratories) and 10^{-3} % solid fluorescent polystyrene particles (Polysciences).

DLS experiments were performed using a set-up as shown in figure 1, specifically using a 35 milli-watt Helium Neon laser (Melles Griot) and a goniometer (Precision Devices) set nominally to measure a 90 degree scattering angle. Measurements were taken for approximately 40 minutes.

DWS experiments were performed using a set-up based on work originally published in [41] and as shown in figure 1. Initially experiments were conducted using a flex99 correlator from correlators.com and a 35 milli-watt Helium Neon laser (Melles Griot). In the quest for

shorter lag times and higher accuracy a flex02 correlator (correlator.com) was purchased. Experiments were first run using water to obtain l^* of the standard solution, and then repeated on the sample solution containing the same phase volume of scatterers. DWS experiments were typically run for approximately 40 minutes to one hour.

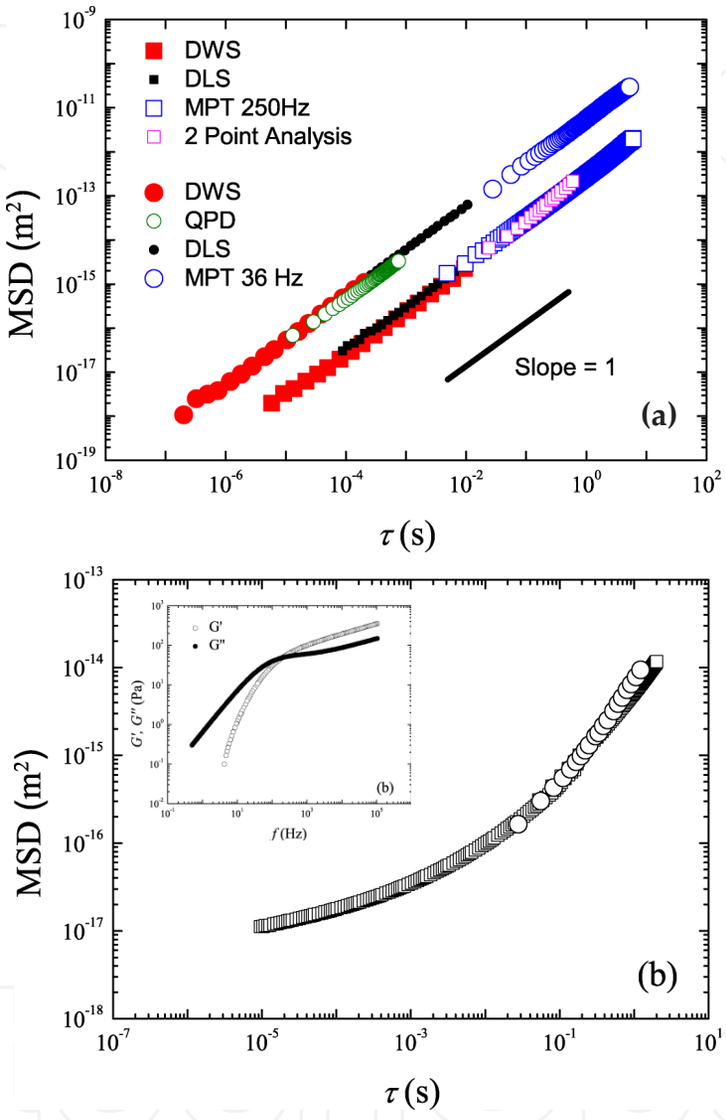

Figure 6. (a) Plot showing the agreement of measurements between multiple techniques in water (circles) and 62% glycerol water mixture (squares). (b) MSD plot for 4 wt% PEO showing an agreement between data obtained using DWS MPT and 2 point analysis (Inset: Extracted rheological properties).

MPT experiments were carried out with an inverted microscope (Nikon Eclipse TE2000-U) on an air damped table (Photon Control) equipped with a mercury fluorescent lamp (X-cite Series 120PC EXFO), and a 60x 1.2 NA (Nikon, Plan Apo VC 60x WI) water immersion objective lens was used for MPT experiments. A range of different cameras were trialled: Foculus FO124SC (CCD), prototype DSI-640-mt smartcam (high speed CMOS), Hamamatsu Orca Flash 2.8 (CMOS large detector size and pixel number). Image series were taken for approxi-

mately ten seconds; and x-y coordinate data extracted using a homebuilt program written using algorithms obtained from: http://physics.georgetown.edu/matlab/. In-house programs to calculate the MSD and Van Hove correlation function were used in combination with a program to extract the rheological information obtained from: http://www.physics.mcgill.ca/~kilfoil/downloads.html.

QPD experiments were also carried out. The microscope used for MPT was additionally utilized to tightly focus a 2 watt 1064 nm Nd:YAG laser (spectra physics) to produce optical traps. Particle displacements were recorded using a 2.5 mW probe laser (Thorlabs S1-FC-675) and a QPD (80 kHz) for approximately 10 seconds. Calibration was aided using piezoelectric multi-axis stage (PI P-517.3CD).

Figure 6(a) shows a log-log plot of the three dimensional mean-square displacement of probe-particles as a function of time; for 500 nm polystyrene particles and 1.86 micron silica beads (optical tweezers data, normalized to 500nm) in either water or a 62 wt% glycerol/water mixture. The mean-square displacement data shown shows an excellent agreement between different methods and also with the expected result of a slope of one (for diffusion in a viscous medium). Figure 6 (b) shows a similar log-log plot of the mean-square displacement versus time for 4 wt%, PEO solutions, together with a fit to a sum of power laws with exponents of ~0.4 and ~0.9, in good agreement with previous work. The inset shows the extracted frequency dependent viscoelastic properties that appear in good agreement with previously published work [14].

2.7. Comparison of with bulk rheometry

The efficiency of these microrheological methods can be assessed against conventional rheometry. Figure 7 reports the elastic modulus *G'* and the loss modulus *G"* for a 30 wt% aqueous dextran solution. G' and G" were obtained using DWS or by the use of a commercial rheometer (TA 2000 rheometer, fitted with a cone-and-plate geometry).

The experimental data were fitted using the Maxwell model:

$$G' = \frac{G_0 \omega^2 \tau^2}{1+\omega^2 \tau^2} \quad ; G' = \frac{G_0 \omega \ \tau}{1+\omega^2 \tau^2} \tag{20}$$

where G_0 is the plateau elastic modulus, τ is the relaxation time, and ω (ω=2 f, f the frequency) the angular frequency. The fit using the Maxwell model allows showing the continuation in the experimental data using the two methods. Further the combination of the two techniques allows the determination of the rheological behaviour over more than 7 decades in frequency. However, at low frequencies, some discrepencies between G' obtained by rheology and the Maxwell model can be observed. This is likely due to the geometry inertia affecting rheological measurements.

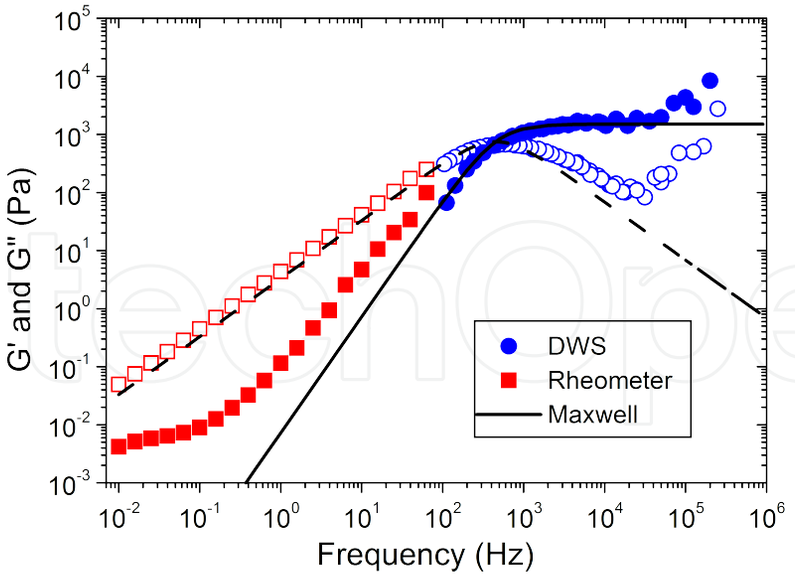

Figure 7. Elastic modulus G′ and loss modulus G″ as a function of frequency for a 30 wt% dextran (500 kDa) in water solution. Experimental data are obtained by conventional rheometry and DWS. Solid lines are a fit using a Maxwell model with one element.

3. Conclusion

The array of microrheology techniques described here provide the ability to measure the viscoelastic properties of a material over approximately nine orders of magnitude in time. The most sensitive technique, DWS, measured particle displacements to nanometre resolution, while MPT could measure the largest displacements, on the order of micrometres. Each technique can be used to measure the mechanical properties of both viscous and viscoelastic materials and has a promising future in experimental biophysics.

Author details

Bradley W. Mansel[1], Stephen Keen[1,2], Philipus J. Patty[1], Yacine Hemar[2,3] and Martin A.K. Williams[1,2,4]

1 Institute of Fundamental Sciences, Massey University, Palmerston North, New Zealand

2 MacDiarmid Institute for Advanced Materials and Nanotechnology, New Zealand

3 School of Chemical Sciences, University of Auckland, New Zealand

4 Riddet Institute, Palmerston North, New Zealand

References

[1] MacKintosh FC, Schmidt CF. Microrheology. Current Opinion in Colloid & Interface Science, 1999; 4 (4) 300-307.

[2] Gardel ML, Valentine MT, Weitz DA. Microscale diagnostic techniques. Springer, 2005.

[3] Yamada S, Wirtz D, Kuo SC. Mechanics of living cells measured by laser tracking microrheology. Biophysical journal 2000; 78 (4) 1736-1747.

[4] Tseng Y, Lee JSH, Kole TP, Jiang I, Wirtz D. Micro-organization and visco-elasticity of the interphase nucleus revealed by particle nanotracking. Journal of Cell Science. 2004; 117 (10):2159-2167. doi:10.1242/jcs.01073.

[5] Duits MHG, Li Y, Vanapalli SA, Mugele F. Mapping of spatiotemporal heterogeneous particle dynamics in living cells. Physical Review E 2009; 79 (5). doi:10.1103/PhysRevE.79.051910.

[6] Zhu X, Kundukad B, van der Maarel JRC. Viscoelasticity of entangled lambda-phage DNA solutions. Journal of Chemical Physics 2008; 129 (18). doi:185103 10.1063/1.3009249.

[7] Ji L, Loerke D, Gardel M, Danuser G. Probing intracellular force distributions by high-resolution live cell imaging and inverse dynamics. In: Wang YLDDE (ed) Cell Mechanics, vol 83. Methods in Cell Biology 2007, pp 199-+. doi:10.1016/s0091-679x(07)83009-3.

[8] Cicuta P, Donald AM. Microrheology: a review of the method and applications. Soft Matter 207; 3 (12):1449-1455. doi:10.1039/b706004c.

[9] Waigh TA. Microrheology of complex fluids. Reports on Progress in Physics 2005; 68 (3):685-742. doi:10.1088/0034-4885/68/3/r04.

[10] Mason TG. Estimating the viscoelastic moduli of complex fluids using the generalized Stokes-Einstein equation. Rheologica Acta 2000; 39 (4):371-378.

[11] Mason TG, Ganesan K, vanZanten JH, Wirtz D, Kuo SC. Particle tracking microrheology of complex fluids. Physical Review Letters 1997; 79 (17):3282-3285. doi:10.1103/PhysRevLett.79.3282.

[12] Pecora R. Dynamic light scattering: applications of photon correlation spectroscopy. Plenum Press, New York, 1985.

[13] Zakharov P, Bhat S, Schurtenberger P, Scheffold F. Multiple-scattering suppression in dynamic light scattering based on a digital camera detection scheme. Applied Optics 2006; 45 (8):1756-1764. doi:10.1364/ao.45.001756.

[14] Dasgupta BR. Microrheology and Dynamic Light Scattering Studies of Polymer Solutions. PhD Thesis; Harvard University, Cambridge, Massachusetts, 2004.

[15] Weitz DA, Pine DJ. Diffusing-wave spectroscopy. In: Brown W (ed) Dynamic Light Scattering: The method and some applications. Oxford University Press, Oxford, 1993; pp 652-720.

[16] Brunel L, Dihang H. Micro-rheology using multi speckle DWS with video camera. Application to film formation, drying and rheological stability. In: Co A, Leal LG, Colby RH, Giacomin AJ (eds) Xvth International Congress on Rheology - the Society of Rheology 80th Annual Meeting, Pts 1 and 2, vol 1027. Aip Conference Proceedings. pp 1099-1101, 2008.

[17] Valentine MT, Kaplan PD, Thota D, Crocker JC, Gisler T, Prud'homme RK, Beck M, Weitz DA. Investigating the microenvironments of inhomogeneous soft materials with multiple particle tracking. Physical Review E 2001; 64 (6). doi:061506 10.1103/PhysRevE.64.061506.

[18] Oppong FK, Rubatat L, Frisken BJ, Bailey AE, De Bruyn, JK. Microrheology and structure of a yield-stress polymer gel. Physical Review E 2006; 73 (4). doi:041405 10.1103/PhysRevE.73.041405.

[19] Kandar AK, Bhattacharya R, Basu JK. Communication: Evidence of dynamic heterogeneity in glassy polymer monolayers from interface microrheology measurements. Journal of Chemical Physics 2010; 133 (7). doi:071102 10.1063/1.3471584.

[20] Gardel ML, Valentine MT, Crocker JC, Bausch AR, Weitz DA. Microrheology of entangled F-actin solutions. Physical Review Letters 2003; 91 (15). doi:158302 10.1103/PhysRevLett.

[21] Valentine MT, Perlman ZE, Gardel ML, Shin JH, Matsudaira P, Mitchison TJ, Weitz DA. Colloid surface chemistry critically affects multiple particle tracking measurements of biomaterials. Biophysical journal 2004; 86 (6):4004-4014. doi:10.1529/biophysj.103.037812.

[22] Crocker JC, Valentine MT, Weeks ER, Gisler T, Kaplan PD, Yodh AG, Weitz DA. Two-point microrheology of inhomogeneous soft materials. Physical Review Letters 2000; 85 (4):888-891.

[23] Levine AJ, Lubensky TC. Two-point microrheology and the electrostatic analogy. Physical Review E 2002; 65 (1). doi:011501 10.1103/PhysRevE.65.011501.

[24] Crocker JC, Hoffman BD. Multiple-particle tracking and two-point microrheology in cells. Cell Mechanics 2007; 83:141-178. doi:10.1016/s0091-679x(07)83007-x.

[25] Sbalzarini IF, Koumoutsakos P. Feature point tracking and trajectory analysis for video imaging in cell biology. Journal of Structural Biology 2005; 151 (2):182-195. doi:10.1016/j.jsb.2005.06.002.

[26] Rogers SS, Waigh TA, Zhao XB, Lu JR. Precise particle tracking against a complicated background: polynomial fitting with Gaussian weight. Phys Biol 2007; 4 (3):220-227. doi:10.1088/1478-3975/4/3/008.

[27] Cheezum MK, Walker WF, Guilford WHQuantitative comparison of algorithms for tracking single fluorescent particles. Biophysical journal 2001; 81 (4):2378-2388.

[28] Savin T. Doyle P.S. Static and dynamic errors in particle tracking microrheology. Biophysical journal 2005; 88 623-638.

[29] Savin T. Doyle P.S. Statistical and sampling issues when using multiple particle tracking. Physical Review E 2007; 76, 021501.

[30] Silburn SA, Saunter CD, Girkin JM, Love GD. Multidepth, multiparticle tracking for active microrheology using a smart camera. Rev Sci Instrum 2011; 82 (3). doi:033712 10.1063/1.3567801.

[31] Keen S, Leach J, Gibson G, Padgett MJ. Comparison of a high-speed camera and a quadrant detector for measuring displacements in optical tweezers. Journal of Optics a-Pure and Applied Optics 2007; 9 (8):S264-S266. doi:10.1088/1464-4258/9/8/s21.

[32] Quan TW, Zeng SQ, Huang ZL. Localization capability and limitation of electron-multiplying charge-coupled, scientific complementary metal-oxide semiconductor, and charge-coupled devices for superresolution imaging. Journal of Biomedical Optics 2010; 15 (6). doi:066005 10.1117/1.3505017.

[33] Carter BC, Shubeita GT, Gross SP. Tracking single particles: a user-friendly quantitative evaluation. Phys Biol 2005; 2 (1):60-72. doi:10.1088/1478-3967/2/1/008.

[34] Czerwinski F, Richardson AC, Oddershede LB. Quantifying Noise in Optical Tweezers by Allan Variance. Optics Express 2009; 17 (15):13255-13269.

[35] Ashkin A. Forces of a single-beam gradient laser trap on a dielectric sphere in the ray optics regime. Biophysical journal 1992; 61 (2):569-582.

[36] Svoboda K, Block SM. Biological applications of optical forces. Annual Review of Biophysics and Biomolecular Structure 1994; 23:247-285. doi:10.1146/annurev.bb.23.060194.001335.

[37] Keen S. High -Speed Video Microscopy in Optical Tweezers. PhD Thesis. University of Glasgow, Glasgow, 2009.

[38] Dufresne ER, Spalding GC, Dearing MT, Sheets SA, Grier DG. Computer-generated holographic optical tweezer arrays. Rev Sci Instrum 2001; 72 (3):1810-1816.

[39] Curtis JE, Koss BA, Grier DG. Dynamic holographic optical tweezers. Optics Communications 2002; 207 (1-6):169-175.

[40] Molloy JE, Padgett MJ. Lights, action: optical tweezers. Contemporary Physics 2002; 43 (4):241-258. doi:10.1080/00107510110116051.

[41] Hemar Y, Pinder DN, Hunter RJ, Singh H, Hebraud P, Horne DS. Monitoring of flocculation and creaming of sodium-caseinate-stabilized emulsions using diffusing-wave spectroscopy. Journal of Colloid and Interface Science 2003; 264 (2):502-508. doi:10.1016/s0021-9797(03)00453-3.

IntechOpen